J Mater Sci (2009) 44:5743–5753
DOI 10.1007/s10853-009-3805-0

Surface changes during pyrolytic conversion of hybrid materials to oxycarbide glasses

A. Tamayo · L. Téllez · R. Peña-Alonso · F. Rubio · J. Rubio

Received: 29 April 2009 / Accepted: 11 August 2009 / Published online: 26 August 2009

Abstract Hybrid materials from TEOS–TBOT–PDMS have been prepared and pyrolyzed between 400 and 1,000 °C. The surface characteristics of this type of materials have been studied by nitrogen adsorption, mercury intrusion porosimetry, and inverse gas chromatography at infinite dilution (IGC). IGC has been used for obtaining the dispersive and acid–base surface energies of the different materials. The specific surface areas and pore volumes of the studied samples have resulted to increase the pyrolysis temperatures ranging between 400 and 600 °C and decrease for higher temperatures. On the other hand, surface energies increase when the materials are pyrolyzed between 400 and 800 °C and then decrease after pyrolysis at 1,000 °C. When the material is pyrolyzed at the highest temperature, the surface energies are close to that of typical glasses. It has been observed that pyrolyzing at 800 °C the material has the highest values of both components of the surface free energy (dispersive and specific). The surface energy–pyrolysis temperature variation does not correspond to the formation of micropores in the material during the pyrolysis process. Therefore, it has been assumed that high energy active sites must be formed on the surface when the materials are pyrolyzed at 800 °C.

A. Tamayo (✉)
Technische Universität Darmstadt, Institut für Materialwissenschaft, Petersenstrasse 23, 64287 Darmstadt, Germany
e-mail: tamayo@materials.tu-darmstadt.de

L. Téllez
ESIQIE-Instituto Politécnico Nacional, UPALM-Zacatenco, 07738 Mexico, DF, Mexico

R. Peña-Alonso · F. Rubio · J. Rubio
Instituto de Cerámica y Vidrio, CSIC, c/Kelsen, n° 5, Campus de Cantoblanco, 28049 Madrid, Spain

Introduction

During the last years a great effort to prepare and characterize silicon oxycarbide glasses through pyrolysis of hybrid materials in inert atmosphere has been carried out [1]. The hybrid materials can be synthesized by the sol–gel process. In this process, organically modified alkoxysilanes are hydrolyzed and condensed to form a hybrid structure where oxygen and carbon functionalities on the silicon are maintained during the whole process. To prepare silicon oxycarbide glasses it is required to pyrolyze the hybrid materials at temperatures around 1,000 °C. During the pyrolysis treatment different reactions such as redistribution reactions, decomposition of organic groups, dehydrogenation, and cross-link of terminal organic groups occur [1, 2].

Silicon oxycarbide glasses are characterized by the presence of Si–O and Si–C bonds forming amorphous mixed SiC_zO_{4-z} ($0 \leq z \leq 4$) units which built up a network with the stoichiometry $SiC_xO_{2(1-x)}$ ($0 \leq x \leq 2$) [3]. In this ideal network no Si–Si, C–O, and C–C bonds exist. However, in most of the silicon oxycarbide glasses a fraction of carbon has been shown to appear as free carbon (C_{free}) in a nanostructured phase [1]. Therefore, the overall composition of SiCO glasses can be expressed as $SiC_xO_{2(1-x)} + {}_yC_{free}$. In accordance with this proposed structure, some carbidic units [$C(Si)_4$] are formed in silicon oxycarbide glasses, leading to the strengthening of the network. As a result, the properties directly related to the structure such as elastic modulus, hardness, strength, resistance to devitrification, etc. are improved.

Silicon oxycarbide glasses are commonly synthesized through controlled pyrolysis of preceramic precursors such as polysiloxanes, polycarbosilanes, and hybrid organic–inorganic materials. As it has been mentioned before, this

kind of hybrid materials can be prepared through the sol–gel process by the polycondensation of alkoxysilanes and alkylalkoxysilanes in alcoholic medium using acidic water as catalyst [1–5]. Recently, hybrid materials prepared from polysiloxanes and alkoxysilanes and alkoxyborates have been used as precursors of silicon and silicon–boron oxycarbide glasses, respectively [2, 4, 5]. The main advantage of polysiloxanes concerns their stability in air as they are thermally stable up to 500 °C [2].

Silicon oxycarbide glasses have been obtained both, as dense and porous microstructure materials [1–13]. When dense oxycarbide glasses are obtained, their mechanical properties are improved over those of vitreous silica. Values for elastic modulus of 115 GPa, flexural strength of 550 Mpa, and Vickers hardness of 9 GPa have been reported [10]. On the other hand, porous oxycarbide glasses can be divided into microporous and/or mesoporous materials. Microporous oxycarbide glasses show specific surface areas (SSA) higher than 200 $m^2\ g^{-1}$ [11]. These surface areas have been retained even at 1,200 °C. At the same time, periodic mesoporous oxycarbide glasses may be obtained with 2D-hexagonal porous structures of 4 nm of average pore size and 200 $m^2\ g^{-1}$ of SSA [12]. Porosity can be obtained during the preparation procedure or by HF etching [14]. Furthermore, it is possible to obtain a wide range of porosities in the same silicon oxycarbide glass [13] and even to grow carbon nanotubes inside the pore microstructure of this type of glasses [15].

The pyrolysis process of hybrid materials have been studied by different techniques such as ^{29}Si solid state NMR and FT-IR spectroscopies [8, 16, 17], thermogravimetric analysis coupled to mass spectrometry (TG/MS) [18], XRD [19, 20], TEM [11, 19], SEM [10, 20, 21], nitrogen adsorption, and mercury intrusion porosimetry [20, 21]. However, as far as we know, the surface energy changes that occur when the organic–inorganic hybrid material is transformed to an inorganic network have not been studied yet. Thus, it is the purpose of this work analyzing the surface changes occurring in this type of materials during their pyrolysis treatment.

Experimental procedure

A hybrid material was prepared starting from tetraethylorthosilicate (TEOS), tetrabutylorthotitanate (TBOT), and hydroxyl terminated dimethyl polysiloxane (PDMS) of 1,750 g mol^{-1}. The weight ratios (TEOS + TBOT)/PDMS and TBOT/TEOS were 60/40 and 7/93, respectively. In the sol–gel reaction, isopropanol was used as solvent, H_2O as hydrolyzing agent, and HCl as catalyst with the following molar ratios: isopropanol/(TEOS + TBOT) = 4/1, H_2O/(TEOS + TBOT) = 3/1, and HCl/(TEOS + TBOT) = 0.3. The reaction was carried out as follows: the corresponding amounts of TEOS, PDMS, and 1/3 of isopropanol were mixed into a vessel thermostatized at 80 °C. After a vigorous stirring for 60 min, a solution with the corresponding amounts of H_2O, HCl, and 1/3 of isopropanol was rapidly added. The new solution was then stirred for 5 min at the same temperature. Then, the solution containing the corresponding amount of TBOT and 1/3 of isopropanol was added drop-wise for about 20 min to avoid the precipitation of TBOT. After 5 min of vigorous stirring at the same temperature, the resulting sol was poured into a plastic container and sealed until gelification. The gel was maintained sealed for 7 days, and after that the exuded liquid was removed daily. Finally, the hybrid xerogel was dried at 50 and 100 °C until not weight loss was observed. The dried hybrid was pyrolyzed at 400, 600, 800, and 1,000 °C in an electrical oven using a pure and dried nitrogen atmosphere. The heating rate used during pyrolysis was 5 °C min^{-1}, and for each treatment the material was maintained for 2 h at the maximum temperature. Monoliths were obtained for all pyrolyzed samples, which were stored in a desiccator until used.

Pyrolyzed samples were analyzed by nitrogen gas adsorption, mercury intrusion porosimetry, and inverse gas chromatography (IGC). To avoid particle size effects any pyrolyzed sample was grinded in an agate mortar and sieved with Teflon mesh. Particles sized between 0.2 and 0.3 mm were used for any experimental analysis. Nitrogen adsorption–desorption isotherms were analyzed with a TriStar 3000 (Micromeritics Instrument Corp., Norcross, GA) in all the partial pressure range at 77 K. Samples were previously degassed at 150 °C during 20 h. The pore size distributions were obtained from the adsorption isotherms using the Barrett–Joyner–Halenda (BJH) method in the pore range between 2 and 50 nm [22]. The specific surface areas were evaluated using adsorption data in the relative pressure range from 0.05 to 0.3 and the Brunauer–Emmet–Teller (BET) equation [23].

For Hg porosimetry measurements, an Autopore II 9215 (Micromeritics Instrument Corp., Norcross, GA) was used in the range of pressures between 0.5 and 410 MPa. The samples were outgassed below 6.67 Pa at room temperature before measurements.

IGC measurements were carried out at infinite dilution using a gas chromatograph (Perkin Elmer, Autosystem) fitted with a flame ionization detector (FID). Thirty centimeters long tubing packed with the corresponding pyrolyzed particles were used. The flow rate of the carried gas (He) was fixed at 20 $cm^3\ min^{-1}$ and, before the measurements, the columns were conditioned at 150 °C for 20 h. The temperature of the injector and detector was set to 180 °C. The signal of the FID was analyzed using a GC integrator (Perkin Elmer Nelson). IGC at infinite dilution

Table 1 Probes used to characterize the surface energy of hybrid materials

Probes	Abbreviation	DN (kcal mol^{-1})	AN	Character	$(hv)^{1/2}\alpha_o 10^{49}$ ($C^{3/2}$ m^2 $V^{-1/2}$)
n-Pentane	C5	–	–	Neutral	8.1
n-Hexane	C6	–	–	Neutral	9.2
n-Heptane	C7	–	–	Neutral	10.3
n-Octane	C8	–	–	Neutral	11.45
Chloroform	CL	0	23.1	Acid	7.8
Benzene	BZ	0.1	8.2	Acid	8.6
Acetone	AC	17.0	12.5	Amphoteric	5.8
Ethyl acetate	EA	17.1	9.3	Amphoteric	7.9
Diethyl ether	DE	19.2	3.9	Base	7.3
Tetrahydrofuran	THF	20.0	8.0	Base	6.8

was achieved using a 1 μL Hamilton syringe. At least five experimental injections were carried out for any probe used at the measurement temperatures of 60, 70, and 80 °C. Different organic probes were used as indicated in Table 1.

IGC at infinite dilution

IGC consists of injecting independently different gas probes into a chromatographic column packed with a stationary solid phase of unknown surface properties. The condition of infinite dilution is reached when the amount of the injected probe is at the limit of detection of a high sensitive detector. Under these conditions, the retention volume, V_N, is not affected by changes in powder mass, flow rate or injected amount [24–27] and is only influenced by the surface properties of the stationary phase under investigation. Therefore, V_N can be computed from the following equations [28]:

$$V_N = F \cdot J(t_R - t_o) \quad (1)$$

$$J = 3/2\left((P_i/P_o)^2 - 1\right)\Big/\left((P_i/P_o)^3 - 1\right) \quad (2)$$

where F is the carrier gas flow, J is the James-Martin gas compressibility factor, t_o is the retention time of a non-adsorbed gas, t_R is the retention time of the gas probe at the measurement temperature, and P_i and P_o are the inlet and outlet pressures of the carrier gas, respectively.

When the condition of infinite dilution is achieved, the adsorption of a probe on a solid surface is expressed by the molar adsorption free energy, ΔG_A, which can be calculated as follows [29]:

$$\Delta G_A = RT \ln(V_N/(S_S W)) + C \quad (3)$$

where R is the ideal gas constant, S_S is the specific surface area of the solid, W is the sample weight in the chromatographic column, and C is a constant which depends on the reference state of the probe. When probes with different properties are injected, the corresponding ΔG_A values can be used for characterizing the surface free energy, γ_S, of the solid as it will be shown below. It is well accepted that γ_S can be split into two terms, as follows:

$$\gamma_S = \gamma_S^d + \gamma_S^{SP} \quad (4)$$

where γ_S^d and γ_S^{SP} are the non-specific (dispersive) and specific (acid–base) components of the surface free energy, respectively. This approach was given by Fowkes to evaluate surface thermodynamics by IGC [26]. In Eq. 4, both dispersive and specific components of the surface free energy must be calculated by using non-specific and specific probes, respectively. The determination of such surface components will be detailed below.

Dispersive component of the surface free energy

When non-polar probes are injected into the chromatographic column, only dispersive interactions are taken place and, therefore, the second term of Eq. 4 is zero. Then, the dispersive component of the solid surface free energy (γ_S^d) can be determined according to the following equation [25]:

$$\gamma_S^d = \left(1/\left(4\gamma_{(-CH_2-)}\right)\right)\left(\Delta G_{A(-CH_2-)}/\left(N_A a_{(-CH_2-)}\right)\right)^2 \quad (5)$$

where N_A is the Avogadro number, $a_{(-CH_2-)}$ is the area occupied by a methylene (–CH_2–) group (0.06 nm^2), $\Delta G_{A(-CH_2-)}$ is the adsorption free energy of a –CH_2– group, and $\gamma_{(-CH_2-)}$ is the surface energy of a solid entirely made of –CH_2– groups. The variation of $\gamma_{(-CH_2-)}$ with temperature is given by $\gamma_{(-CH_2-)} = 35.6 - 0.058$ $(T - 293)$ (in mJ m^{-2} K^{-1}). $\Delta G_{A(-CH_2-)}$ is calculated according to:

$$\Delta G_{A(-CH_2-)} = -RT\ln\left(V_{N,n}/V_{N,n+1}\right) \quad (6)$$

where $V_{N,n}$ and $V_{N,n+1}$ denote the retention volumes of *n*-alkanes having n and $n + 1$ atoms, respectively.

Evaluation of the specific (acid–base) interaction components

If polar probes are injected into the chromatographic column, both dispersive and specific interactions are established between these probes and the stationary solid surface. Then, the specific component of the free adsorption energy is determined from the difference between adsorption energy of the polar probe and its dispersive increment. Such difference is carried out in accordance with the method of Saint Flour and Papirer [30] who proposed to use *n*-alkane probes as references because only interact through dispersive forces. According to these authors,

$$\Delta G_i^{\mathrm{SP}} = \Delta G_i - \Delta G_i^{\mathrm{d}} = -RT\ln\left(V_{\mathrm{N},i}/V_{\mathrm{N,ref}}\right) \quad (7)$$

where ΔG_i, ΔG_i^{SP}, and ΔG_i^{d} denote the free adsorption energy and its specific and dispersive component, respectively, determined for the test probe; $V_{\mathrm{N},i}$ and $V_{\mathrm{N,ref}}$ refer to net retention volumes of the test probe and an hypothetical *n*-alkane, respectively, and *i* denotes the consecutive test probe.

The problem to use this method consists in choosing a reference probe property reflecting the ability of probe molecules to undergo dispersive interactions with the solid surface. Several methods have been proposed in the literature using different reference properties [31]. In this work $(hv)^{1/2}\alpha_0$ have been used, being hv the ionization potential of the probe and α_0 its molecular induction polarizability. Donnet et al. [32] have proved this property to be useful for characterizing carbon blacks, active carbons, and carbon fibers obtained from pyrolysis of organic polymers [32, 33].

When ΔG_i^{SP} is obtained for any polar probe, then it is possible to calculate the specific component of enthalpy of adsorption, ΔH_i^{SP}, from the temperature dependence of ΔG_i^{SP} [34]. The enthalpy of specific interactions between the examined solid surface and test probe is calculated from the acid–base properties of both the surface and the probe molecule which are expressed as follows:

$$-\Delta H^{\mathrm{SP}} = k_{\mathrm{D}}\mathrm{AN} + k_{\mathrm{A}}\mathrm{DN} \quad (8)$$

where AN and DN denote acceptor and donor number of the test probe, respectively, and k_{A} and k_{D} are the parameters describing the ability of the examined surface to act as electron acceptor and donor.

The donor number DN (kJ mol^{-1}) is a measure of Lewis basicity [35] being defined as the negative molar enthalpy of the reaction between the examined base (donor) and a standard Lewis acid $SbCl_5$ (acceptor) in 10^{-3} M 1,2-dichloroethane solution. The acceptor number, AN, is determined from the relative chemical shift in ^{31}P-NMR triethylophosphine oxide (standard donor) dissolved in the examined acceptor and is expressed as a dimensionless quantity in conventional units (0 = hexane, 100 = 1,2-dichloroethane). DN and AN values and other probe characteristics are given in Table 1.

Results

Pore size distributions (PSDs) and specific surface areas (SSA)

Figure 1 shows the nitrogen adsorption–desorption isotherms for the as-prepared and pyrolyzed materials. In accordance with the IUPAC classification, the isotherms of the as-prepared samples and samples pyrolyzed at 400 and 1,000 °C were type IV whereas that of sample pyrolyzed at 800 °C was type I [36]. The sample pyrolyzed at 600 °C showed an isotherm type between I and IV according to the IUPAC isotherms classification. The type IV isotherms showed very small hysteresis loops as an indication of the presence of small porosity in the range from 2 to 50 nm, i.e., low concentration of mesopores in accordance with IUPAC. However, as it will be commented in next paragraphs, these samples may also have micropores, i.e., pores below 2 nm, which do not produce hysteresis loops. On the other hand, for the sample pyrolyzed at 800 °C the type I isotherm, or Langmuir isotherm, correspond to a microporous solid. A similar isotherm has been obtained for SiTiOC oxycarbide glasses [37]. Finally, the hybrid material heat treated at 600 °C showed a small hysteresis loop on the isotherm, revealing that this sample is mainly microporous with some contribution of mesopores.

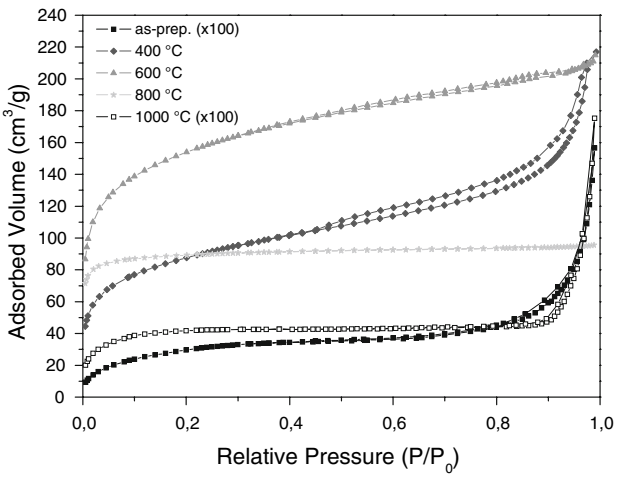

Fig. 1 Nitrogen gas adsorption–desorption isotherms of TEOS–TBOT–PDMS hybrid and pyrolyzed materials. (Notice that the isotherms corresponding the as-prepared and 1,000 °C pyrolyzed material have been multiplied by 100)

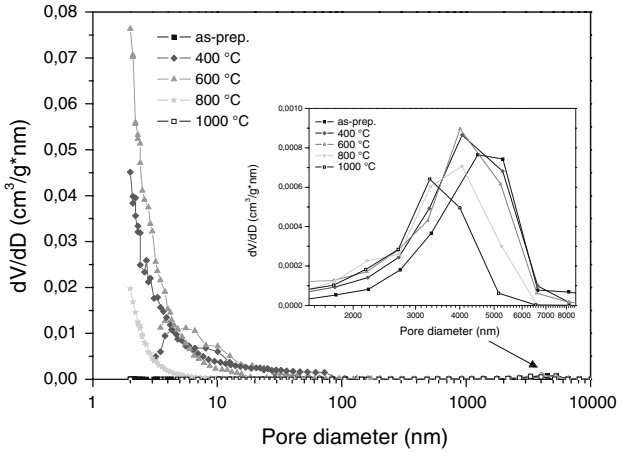

Fig. 2 Pore size distributions of hybrid and pyrolyzed materials

As long as nitrogen sorption isotherms only give information concerning micro- and mesopores, the presence of macropores (i.e., pores between 500 nm and 0.3 mm) must be determined by mercury intrusion porosimetry. Figure 2 shows the corresponding pore size distributions (PSDs) for the as-prepared and pyrolyzed samples for the mesopore and macropore size ranges. The peak in the PSDs corresponding to the macropore range decreases with the pyrolysis temperature. The as-prepared hybrid material presents a maximum peak at 4.7 μm, and for the samples pyrolyzed at 400, 600, 800, and 1,000 °C such peak appears at 4.4, 4.3, 3.9, and 3.5 μm, respectively. This decrease with pyrolysis temperature is due to the shrinkage process during heating. On the other hand, the intensity of this peak increases from the as-prepared material to that pyrolyzed at 400 and 600 °C, and then decreases for higher pyrolysis temperatures. This result indicates that at 600 °C the pyrolyzed sample has the highest macropore volume whereas it decreases for higher pyrolysis temperatures.

In the mesopore range the PSDs show a continuous increase of pore volume from 10 to 2 nm. This behavior indicates that all samples contain mesopores and micropores. The presence of microporosity can be assessed by means of the V–α_s plot [38]. All V–α_s plots (not shown here) presented a straight region over a wide α_s range and finally a downward deviation indicating the presence of microporosity for both as-prepared and pyrolyzed samples. The high downward deviation for the samples pyrolyzed at 600 and 800 °C constitutes an indication of high concentration of micropores. From the downward deviation it is possible to fit a straight line and the Y-axes intercept corresponds to the micropore volume of the analyzed sample.

Table 2 displays the pore volumes and pore sizes obtained for the as-prepared and pyrolyzed samples. The as-prepared and samples pyrolyzed at 400, 600, and 800 °C show micro-, meso-, and macropores, whereas when pyrolysis is carried out at 1,000 °C the disappearance of the micropores occurs together with a significant shrinkage of the sample. It is also observed that the as-prepared hybrid material has mainly macropores, a result that is similar to that obtained by Chung et al. [39] and Guo et al. [40]. Mesopores are present when the pyrolysis is carried out at 400 and 600 °C due to the loss of gases formed during thermal redistribution reactions [2, 18]. Micropores appear at 400 °C but their highest concentration occurs at 600 and 800 °C. Micropores must be originated by the same facts that those forming mesopores but also by the shrinkage process of mesopores which decrease in size up to the range of micropores. This later result can be observed in Fig. 2 and shows that the as-prepared hybrid material and those pyrolyzed at 400, 600, and 800 °C develop multiple size-scale morphologies, ranging from nanometers to micrometers in accordance with Guo et al. [41].

SSA has been calculated for all the samples. Mesopore SSAs were obtained from the BHJ method, macropore SSAs were obtained from mercury porosimetry, and micropore SSAs were obtained by subtraction of macropore and mesopore SSAs from BET. In Table 3 the SSAs for all the studied samples are collected. The same trend of the previously mentioned pore volumes is observed, however, the higher contribution to the total SSA is given by the mesopores but mainly by the micropores.

Dispersive surface energy

The effect of pyrolysis temperature on the dispersive and acid–base properties of TEOS–TBOT–PDMS hybrid

Table 2 Average pore size and pore volume values of as-prepared and pyrolyzed TEOS–TBOT–PDMS materials

Sample	Mean pore size (nm)		Pore volume ($cm^3\ g^{-1}$)			
	Micro–meso ± 0.03	Macro ± 20	Micro ± 0.008	Meso ± 0.006	Macro ± 0.2	Total ± 0.2
As-prepared	9.13	4695	0.001	0.003	1.7	1.7
400 °C	4.47	4442	0.082	0.230	2.5	2.8
600 °C	2.57	4352	0.174	0.185	2.4	2.7
800 °C	2.08	3928	0.132	0.026	1.5	1.7
1,000 °C	8.03	3498	0	0.002	1.1	1.1

Table 3 Specific surface area values of as-prepared and pyrolyzed TEOS–TBOT–PDMS materials

Sample	SSA ($m^2\ g^{-1}$)			
	Micropores	Mesopores	Macropores	Total
As-prepared	0.4 ± 0.1	0.5 ± 0.1	0.1 ± 0.1	1.1 ± 0.1
400 °C	123.3 ± 5	151.7 ± 5	25.0 ± 2	300.1 ± 7
600 °C	286.4 ± 7	193.9 ± 6	34.8 ± 2	515.2 ± 7
800 °C	239.9 ± 7	41.1 ± 2	2.0 ± 0.5	283.1 ± 7
1,000 °C	0	0.3 ± 0.1	1.1 ± 0.1	1.4 ± 0.1

materials has been studied from IGC measurements. Dispersive properties have been obtained from the variation of the net retention volume of the *n*-alkanes against the carbon atom number of the probe. Figure 3 displays the representation of the net retention volume vs. the carbon atom number of the probe for the as-prepared and pyrolyzed hybrid samples.

It is noticed in this figure that net retention volumes can be well fitted with straight lines respect to the carbon atom number of the probes. Regression coefficients of all straight lines have been always higher than 0.9995. From the slopes of that lines the free energy of adsorption of one $–CH_2–$ group, $\Delta G_{A(-CH_2-)}$, has been obtained for each sample. Dispersive components of the surface energy have been then calculated from Eq. 5. Table 4 gives the γ_S^d values for the as-prepared hybrid sample pyrolyzed at different temperatures.

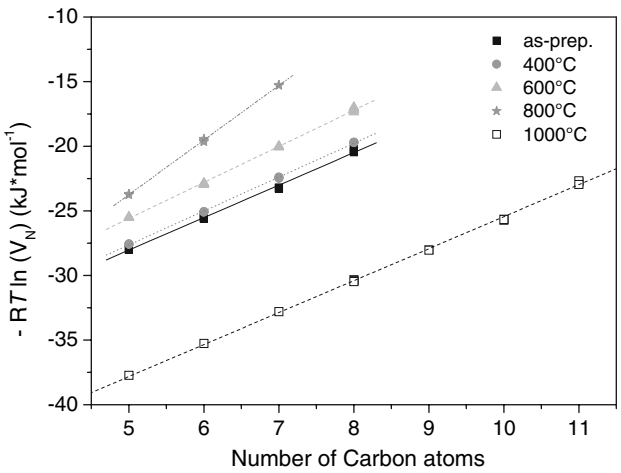

Fig. 3 Net retention volume of *n*-alkanes versus number of carbon atoms of the probes for the as-prepared and pyrolyzed materials at 80 °C

Table 4 shows that γ_S^d values decrease with the measurement temperature, a result which indicates that the intermolecular interactions of the different probes with the studied sample surfaces are of physical nature [25]. From these results it is possible to determine both entropic (s_s^d) and enthalpic (h_s^d) dispersive components of the surface free energy of the solids in accordance with Eq. 9. These values are also given in Table 4

$$\gamma_S^d = h_s^d + Ts_s^d \tag{9}$$

In Table 4 the entropic contribution is expressed as the percentage of the corresponding dispersive surface energy. Therefore, the influence of the temperature for the studied materials can be quantified using the relative temperature gradient of γ_S^d expressed as percentage.

The γ_S^d value obtained for the as-prepared hybrid material is consistent with those of the respective molecules which are forming it. Thus, for PDMS Pérez et al. [42] predicted a value of 21.31 mJ m^{-2} for γ_S^d. Rubio et al. [41] obtained values between 60 and 80 mJ m^{-2} for γ_S^d for silica xerogels heat treated between 700 and 900 °C. On the other hand, for silica–TEOS–PDMS hybrid materials, Martos et al. [43] obtained γ_S^d values ranging from 31 to 58 mJ m^{-2} depending on the type of silica (Aerosil) used for preparing the hybrid. Finally, Bogillio et al. found values of 28.60, 43.14, and 44.90 mJ m^{-2}, respectively, for SiO_2, TiO_2, and SiO_2–TiO_2 materials [44].

The average γ_S^d value obtained in this work for the as-prepared hybrid sample (40.55 mJ m^{-2}) is higher than that of PDMS but lower than those of heat treated silica xerogels and very close to that of TiO_2, showing that the hybrid surface must be considered as a nanocomposite of silica, TiO_2, and PDMS molecules. If PDMS molecules were covering the whole hybrid surface, then the outcoming

Table 4 Dispersive components of surface energy of as-prepared and pyrolyzed TEOS–TBOT–PDMS materials

Sample	γ_S^d (mJ m^{-2}) ± 1.3			Average γ_S^d (mJ m^{-2}) ± 1.3	$-(d\gamma_S^d/dT)/\gamma_S^d$ (%)	h_s^d (mJ m^{-2}) ± 1.3
	Measurement Temp.					
	60 °C	70 °C	80 °C			
As-prepared	47.14	40.51	34.00	40.55	1.62	86.54
400 °C	47.29	42.34	36.98	42.20	1.22	78.29
600 °C	50.38	47.17	41.96	46.50	0.90	75.97
800 °C	124.81	117.97	106.48	116.42	0.78	180.58
1,000 °C	57.72	51.34	45.17	52.08	1.20	95.33

value would be close to that of PDMS. The obtained value indicates that PDMS molecules are well distributed over all the hybrid structure and not only on the surface. Therefore, the structure of the hybrid TEOS–PDMS–TBOT material must be similar to that proposed by Chung et al. [39] and Babonneau [45] in which silica–titania primary particles are bonded by PDMS molecules, but not all the primary particle surfaces are bonded to PDMS molecules.

Results of Table 4 display γ_S^d values similar to the obtained for other hybrid or glass materials except those values obtained for the sample pyrolyzed at 800 °C [43, 46]. This sample shows very high γ_S^d values which indicate a very high surface energy. This result must be associated to the presence of highly active sites on the pyrolyzed surface. At the same time, this sample exhibits the lowest relative temperature gradient of γ_S^d as an indication that the interactions are so strong that they slightly change with temperature.

Acid–base (k_A, k_B) surface properties of the hybrid materials

The effect of the pyrolysis temperature on the acid–base properties of TEOS–PDMS–TBOT hybrid materials has been also obtained from IGC measurements. When polar probes are injected into the chromatographic column, both dispersive and specific interactions are established between the probes and the solid surface. To separate dispersive interactions from specific ones, it is necessary to plot the adsorption free energy ($-\Delta G_A$) of polar and non-polar probes versus a physico-chemical property reflecting the ability of such probes to undergo dispersive interaction with the surface sites. All non-polar probes lie on a straight line and polar ones lie above this line. Differences of ordinates between the point corresponding to any polar probe and the straight line correspond to specific interaction contributions ($-\Delta G_A^{SP}$) in which the dispersive contributions have been eliminated. In this work, adsorption free energies ($-\Delta G_A$) of polar and non-polar probes have been plotted versus the physico-chemical property molecular induction polarizability, $(h\nu_L)^{1/2}\alpha_L$ [32]. Figures 4 and 5 display these representations for the hybrid samples pyrolyzed at 400 and 800 °C, respectively, at the measurement temperature of 80 °C. It is observed that all non-polar probes fall on a straight line whereas polar probes deviate from this line. From such deviations $-\Delta G_A^{SP}$ values are obtained.

The bar diagram on Fig. 6 representing the $-\Delta G_A^{SP}$ values for different specific probes interacting with as-prepared and pyrolyzed samples reveal the dependance of ΔG_A^{SP} on two factors: the acid–base behavior of the polar probes, determined by their donor (DN) and acceptor (AN) numbers, and on their $(h\nu)^{1/2}\alpha_0$ value respect to those of

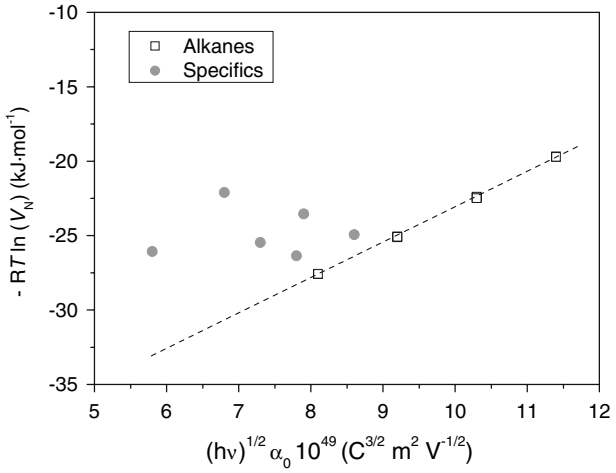

Fig. 4 $RT\ln(V_N)$ versus $(h\nu)^{1/2}\alpha_0$ (molecular induction polarizability) plot for the 400 °C pyrolyzed sample, at 80 °C

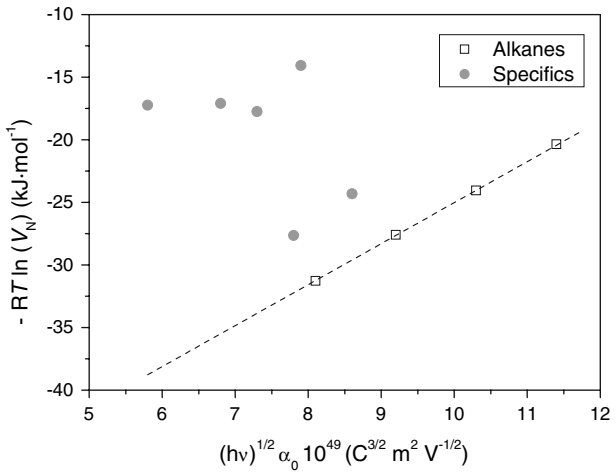

Fig. 5 $RT\ln(V_N)$ versus $(h\nu)^{1/2}\alpha_0$ (molecular induction polarizability) plot for the 800 °C pyrolyzed sample, at 80 °C

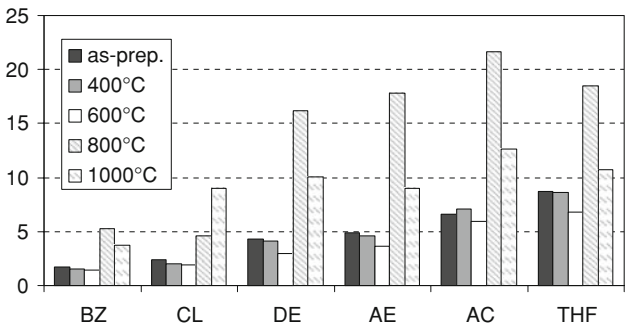

Fig. 6 Specific surface free energy (ΔG_A^{SP}, kJ mol^{-1}) values for the as-prepared hybrid and pyrolyzed materials

n-alkanes. Thus, acidic probes give the lowest ΔG_A^{SP} values and, on the other hand, THF and acetone probes give the highest values due to their higher AN and DN numbers.

This behavior shows that both acid and base active sites exist on the surface of hybrid and pyrolyzed materials.

Figure 6 shows that the as-prepared samples and those pyrolyzed at 400 and 600 °C exhibit close values of ΔG_A^{SP}, indicating the organic–inorganic behavior of these materials. On the other hand, the higher ΔG_A^{SP} values of the samples at 800 and 1,000 °C are related to the inorganic character of the materials. In particular the sample pyrolyzed at 800 °C gives the highest values for all the polar probes, a result which is similar to that found for the non-polar or dispersive component of the surface energy given in Table 3.

The ΔG_A^{SP} values are temperature-dependent and contain entropic contributions, therefore if acid–base constants need to be determined then, such contributions must be eliminated. This process can be carried out by analyzing the variation of ΔG_A^{SP} versus the measurement temperature in accordance with the following expression:

$$\Delta G_A^{SP} = \Delta H_A^{SP} - T\Delta S_A^{SP} \quad (10)$$

From this equation ΔH_A^{SP} can be calculated, and acid and base constants of the solid surface, k_A and k_B, can then be determined through Eq. 8 [47].

Table 5 gives the ΔH_A^{SP} values obtained for the as-prepared and pyrolyzed samples. It results that the pyrolysis temperature induces important variations of the surface properties of hybrid samples. This is well illustrated taking, for instance, two probe molecules: a Lewis acid such as chloroform and a base such as diethylether. Clearly, the pyrolysis treatment at 400 and 600 °C decrease the acidic and base properties of the hybrid surface, showing that both acid and base surface sites are removed. Such surface variations must be associated to the gases and low molecular weight molecules evolution during redistribution reactions occurring at these temperatures [18, 48]. However, at the pyrolysis temperature of 800 °C an important increase of ΔH_A^{SP} values for all probe molecules occurred, a result which is also similar to the increase of the dispersive surface energy. Then, it must be concluded that at the pyrolysis temperature of 800 °C an increase in both non-specific and specific surface energies of materials occurs.

Table 5 Enthalpy values, ΔH (kJ mol^{-1} ± 0.10) of hybrid and pyrolyzed materials

Probe	As-prep.	400 °C	600 °C	800 °C	1,000 °C
Benzene	9.38	6.99	5.78	28.24	14.55
Chloroform	17.70	9.15	8.11	26.80	25.79
Ethyl acetate	36.71	29.20	22.13	56.39	28.50
Acetone	38.77	37.07	30.16	80.32	39.09
Diethyl ether	34.97	28.44	20.81	70.06	26.75
Tetrahydrofuran	59.64	41.82	30.28	81.96	47.07

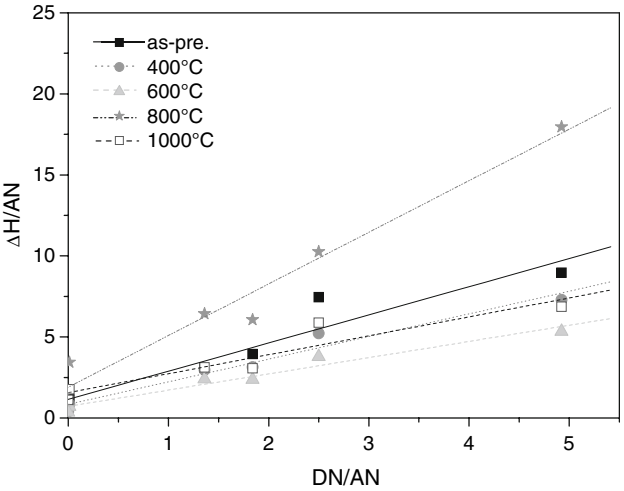

Fig. 7 Experimental determination of acid–base properties of hybrid and pyrolyzed materials

Table 6 Acid–base properties of the hybrid and pyrolyzed materials

Pyrolysis temp (°C)	As-prep.	400 °C	600 °C	800 °C	1,000 °C
k_a ± 0.10	1.73	1.39	0.99	3.18	1.17
k_b ± 0.10	1.15	0.84	0.72	1.91	1.16
k_a/k_b ± 0.10	1.50	1.65	1.37	1.66	1.01

Finally, the ΔH_A^{SP} values of acid probes at the pyrolysis temperature of 1,000 °C increase whereas those of base probes decrease respect to those of the as-prepared hybrid sample. This result now shows that the surface active sites are changing during the pyrolysis process.

Finally, by applying Eq. 8 it is possible to obtain information on the acid–base groups in terms of acceptor and electron donor capacities. In this equation k_A and k_B characterize the surface acidity and basicity for the as-prepared and pyrolyzed hybrid samples (Fig. 7). k_A values are obtained from the slope of the fitting lines and k_B is given by the intercept. The values of k_A, k_B, and the ratio k_A/k_B are displayed in Table 6. These values give a more quantitative importance concerning the strength of either acid or base groups existing on the surface of as-prepared and pyrolyzed hybrid samples.

Discussion

Results of PSDs, pore volumes, and SSAs indicate that both as-prepared hybrid samples and 1,000 °C pyrolyzed materials are mainly macroporous whereas hybrid materials obtained between 400 and 800 °C have a wider range of pore sizes from micro- to meso- and macropores. The meso- and micropores are found as transient porosity

produced during the escape of gases during thermal redistribution reactions [2, 18]. The formation of this transient porosity has been observed for hybrids and pyrolyzed polymers at the same range of pore diameter which have been assigned to the evolution of gaseous compound temperatures [2, 11, 20, 49].

In accordance with PSDs it is observed that the pyrolysis temperature hardly affects macroporosity, and the major effects occur in micro- and mesopores present on the hybrid materials. According to Greil [2], the maximum transient open porosity is observed between 400 and 600 °C, being 400 °C the temperature at which mesopores and macropores density is maxima. At higher temperature, the number of both type of pores decreases. However, microporosity is at 600 °C and then decreases for higher temperatures. These results suggest that micropores are formed by two processes: (a) creation of microporosity due to gas release inside the network, and (b) shrinkage of mesopores by new crosslinking reactions leading to a denser material that transforms the hybrid material in an inorganic one at temperatures close to 800 °C. Finally, at the pyrolysis temperature of 1,000 °C both micro- and mesopores disappear, remaining only the macropores, a result which indicate that this kind of pores can be completely eliminated due to their finer size [20].

The effect of pyrolysis temperature on the dispersive surface free energy has shown a great influence especially at 800 °C (Table 4). The obtained γ_s^d values are consistent with material compositions except for that pyrolyzed at 800 °C. At this temperature the pyrolyzed material has a very high dispersive surface energy. In a previous work we have shown that for hybrid TEOS–TBOT–PDMS materials γ_s^d values are inversely related to the pore diameter [46]. For the pyrolyzed materials studied in this work this relationship is shown in Fig. 8. Pore sizes have been determined for micro- and mesopores ranges assuming that macropores may be considered as external surface. This pore sizes (see Table 2) have been calculated from nitrogen isotherms by using $4V/S$ with V equal to the nitrogen adsorbed volume and S referes the BET specific surface area.

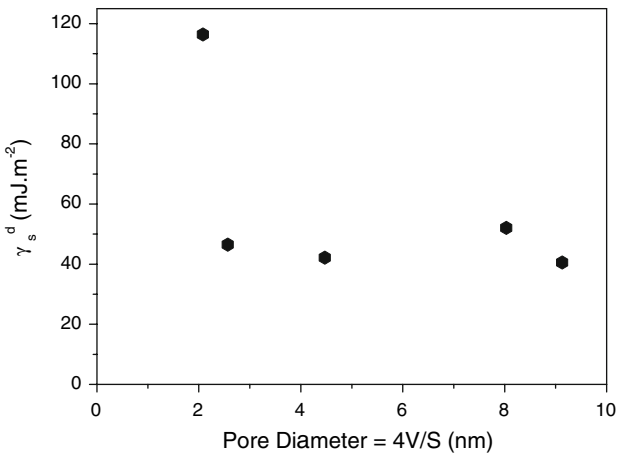

Fig. 8 Variation of the dispersive surface energy (γ_s^d mJ m^{-2}) as a function of the average pore diameter of the samples

Figure 8 shows that there is no correlation between pore size and the average dispersive surface free energy of the as-prepared and pyrolyzed hybrid materials, neither between dispersive surface energy and pore volumes nor specific surface areas. However, if dispersive surface energy is plotted versus pore volumes for the as-prepared and 400 and 600 °C samples, a good fit is possible. Extrapolating to the Y-axes reveals a dispersive surface free energy 55.66 mJ m^{-2}. This value is very close to that obtained in the work for TEOS–TBOT–PDMS hybrid materials equal to 54.53 mJ m^{-2} [46]. This result shows that the surface of the as-prepared hybrid material and 400 and 600 °C pyrolyzed ones are very similar in their chemical nature, whereas hybrids pyrolyzed at 800 and 1,000 °C posses a different chemical behavior.

On the other hand, the γ_s^d value obtained for the hybrid sample pyrolyzed at 1,000 °C is consistent with the values obtained for different glasses, silica, titania, and silica–titania materials even though they are slightly higher. This higher value must be due to the presence of mesopores or some high active sites on the surface of the pyrolyzed material. Such active sites must be responsible for the highest value obtained for the dispersive surface free energy of the hybrid pyrolyzed at 800 °C. However, the value of 116.42 mJ m^{-2} is more than twice of 52.08 mJ m^{-2} of the hybrid pyrolyzed at 1,000 °C, a result which indicates that the active sites of the sample pyrolyzed at 800 °C are always of higher energy. The presence of these high surface energy sites must be assigned to the structural changes occurring when the hybrid organic–inorganic material is transformed to inorganic one. When these transformations occur near 800 °C, several works have reported an unusual strong water adsorption on the pyrolyzed materials [16, 50]. Singh and Pantano [16] have reported that water adsorption occurs on free hydroxyl groups that have been created during the pyrolytic treatment at this temperature. The free hydroxyls may be responsible for the high dispersive surface energy of the material.

If we assume that free surface hydroxyls are the active sites which give the high value of the dispersive surface energy, then the polar component, and more strictly, the acidic polar component of the surface energy, must increase. It is well known that free hydroxyls of Si atoms (silanol groups) are acidic in nature [51], therefore if they are formed on the sample pyrolyzed at 800 °C then, the acidity of the sample must be increased. Results of acid and

base constants, k_A and k_B, of Table 4 show that not only the acid constant increases but also the base constant. This result indicates that both acid and base active sites are formed on the surface of the sample.

Table 4 also reveal that for the as-prepared and 400 and 600 °C pyrolyzed hybrid materials, when the dispersive surface energy increases the specific surface energy, expressed as $k_A + k_B$, decreases. This behavior is consistent with the fact that for most materials the higher ability to polar interactions is associated with the lower ability to dispersive interactions expressed by γ_S^d [34]. The observed results observed indicate that their chemical nature is similar as it has been pointed before. However, this correlation does not exist on 800 and 1,000 °C pyrolyzed samples, but they show that their chemical nature changes during the pyrolytic transformation.

Finally, according to the k_A/k_B ratio values (Table 4) it is observed that all samples are mainly acidic, except that pyrolyzed at 1,000 °C which has an amphoteric surface. The high value of k_A/k_B obtained for the sample pyrolyzed at 800 °C shows that most of the new created active surface sites are acidic at this temperature, a result which is in accordance with the work of Singh et al. [16] showing the formation of free hydroxyls on the surface of pyrolyzed materials. However, it is also well known that the hydroxyl groups are not equally acidic or basic because of the surface heterogeneity [52]. Their functionalities are affected by the number, species, and position of ions surrounding. Besides, TiO_2 and SiO_2–TiO_2 materials are mainly base. For example, Bogillo et al. [44, 53] have reported the surface base character of TiO_2 with values of 1.31 and 2.87 for k_A, k_B, respectively. These later values change to 2.29 and 2.94, respectively, for a SiO_2/TiO_2 sample with 80/20 weight ratio. Therefore, the high base character observed for the 800 °C pyrolyzed sample must be due to the formation of hydroxyl groups on titanium atoms.

This later conclusion for the sample pyrolyzed at 800 °C will be studied in future works to analyze where such high energy acid and base surface sites are formed. Finally, we want to study the benefits of such characteristic, in conjunction with both the high dispersive surface energy and the presence of only microporosity, in technological applications such as membranes, catalysis supports, chromatographic supports, and so on.

Conclusions

In this work the surface characteristics of a TEOS–PDMS–TBOT hybrid material pyrolyzed between 400 and 1,000 °C have been studied. Pore size distributions showed macroporous samples at every studied temperature but meso- and micropores are formed by pyrolysis at 400 °C and remain at 600 °C. Pyrolysis at 800 °C produces the disappearance of mesoporosity whereas pyrolysis at 1,000 °C eliminates the microporosity of the sample. Pore volume and specific surface area of the samples showed a similar trend.

The surface energy of the as-prepared and pyrolyzed materials has been analyzed by means of IGC. The surface energy has been presented as dispersive or non-specific, and as specific or acid–base and both of them are well-correlated with the chemical composition of the studied materials; however, the sample pyrolyzed at 800 °C shows a high energy values for both, dispersive and specific components. This high energy has been attributed to the formation of free hydroxyl groups located on Si and Ti atoms on the surface of the material as both, acid and base specific energies increase.

Acknowledgements This work was supported by the Ministerio de Educación y Ciencia of Spain by the Project Ref. CTQ2006-15692-C02-02 and by the Comunidad de Madrid by the Project S-0505/PPQ/000344. L. Téllez is grateful to the Instituto Politécnico Nacional and the Consejo Nacional de Ciencia y Tecnología (CONACyT) of Mexico for the Grant, Ref. 72432.

References

1. Pantano CG, Singh AK, Zhang H (1999) J Sol-Gel Sci Tech 14:7
2. Greil P (1995) J Am Ceram Soc 78:835
3. Sorarù GD (1994) J Sol-Gel Sci Tech 2:843
4. Wootton AM, Rappensberger M, Lewis MH, Kitchin S, Howes AP, Dupree R (1996) J Non-Cryst Solids 204:217
5. Babonneau F, Bois L, Yang CH, Interrante LV (1994) Chem Mater 6:51
6. Schiavon MA, Redondo SUA, Pina SRO, Yoshida IVP (2002) J Non-Cryst Solids 304:92
7. Martos C, Rubio F, Rubio J, Oteo JL (2003) J Sol-Gel Sci Tech 26:511
8. Peña-Alonso R, Rubio F, Rubio J, Oteo JL (2004) J Anal Appl Pyrol 71:827
9. Flores A, Martos C, Rubio J, Rubio F, Sánchez-Cortés S, Oteo JL (2004) J Am Ceram Soc 87:2093
10. Sorarù GD, Dallapiccola EL, Dándrea G (1996) J Am Ceram Soc 79:2074
11. Singh AK, Pantano CG (1996) J Am Ceram Soc 79:2696
12. Masse S, Laurent G, Babonneau F (2007) J Non-Cryst Solids 353:1109
13. Tamayo A, Rubio J, Peña-Alonso R, Rubio F, Oteo JL (2008) J Eur Ceram Soc 28:1871
14. Dibandjo P, Dirè S, Babonneau F, Sorarù GC (2008) Eur J Glass Sci Technol A 49:175
15. Scheffler M, Greil P, Berger A, Pippel E, Woltersdorf J (2004) Mater Chem Phys 84:131
16. Singh AK, Pantano CG (1997) J Sol-Gel Sci Tech 8:371
17. Gualandris V, Hourlier-Bahloul D, Babonneau F (1999) J Sol-Gel Sci Tech 14:39
18. Belot V, Corriu RJP, Leclercq D, Mutin PH, Vioux A (1992) J Non-Cryst Solids 147&148:52
19. Sorarù GD, D′Andrea G, Campostrini R, Babonneau F, Mariotto G (1995) J Am Ceram Soc 78:379

20. Walter S, Sorarù GD, Bréquel H, Enzo S (2002) J Eur Ceram Soc 22:2389
21. Parmentier J, Sorarù GD, Babonneau F (2001) J Eur Ceram Soc 21:817
22. Barrett EP, Joyner LG, Halenda PP (1951) J Am Chem Soc 73:373
23. Brunauer S, Emmett PH, Teller E (1938) J Am Chem Soc 60:309
24. Planinsek O, Buckton G (2003) J Pharm Sci 92:1286
25. Dorris GM, Gray DG (1980) J Colloid Interface Sci 77:353
26. Fowkes FM (1973) Recent advances in adhesion. Gordon and Breach, New York
27. Voelkel A (2004) Chemom Intel Lab Sys 72:205
28. Conder JR, Young CL (1979) Physicochemical measurements by gas chromatography. Wiley, New York
29. Nardin M, Papirer E (1990) J Colloid Interface Sci 137:534
30. Saint Flour C, Papirer E (1982) Ind Eng Chem Prod Res Dev 21:666
31. Brendle E, Papirer E (1997) J Colloid Interface Sci 194:217
32. Donnet JB, Park SJ, Balard H (1991) Chromatographia 31:434
33. Donnet JB, Park SJ (1991) Carbon 29:955
34. Andrzejewska E, Voelkel A, Andrzejewski M, Maga R (1996) Polymer 37:4333
35. Gutmann V (1979) The donor–acceptor approach to molecular interactions. Plenum, New York
36. Sing KSW, Everett KH, Haul AW, Moscou L, Pierotti RA, Rouquerol J, Siemieniewska R (1985) Pure Appl Chem 57:603
37. Téllez L, Rubio J, Valenzuela MA, Rubio F, Oteo JL (2009) Mater Char 60:506
38. Gregg SJ, Sing KSW (1982) Adsorption surface area and porosity. Academic Press, London
39. Chung YJ, Ting SJ, Mackenzie JD (1990) Mater Res Soc Symp Proc 180:981
40. Guo L, Hyeon-Lee J, Beaucage G (1999) J Non-Cryst Solids 243:61
41. Rubio F, Rubio J, Oteo JL (1997) J Sol-Gel Sci Tech 10:31
42. Pérez E, Schäffer E, Steiner U (2001) J Colloid Interface Sci 234:178
43. Martos C, Rubio F, Rubio J, Oteo JL (2001) J Sol-Gel Sci Tech 20:197
44. Bogillo VI, Voelkel A (1997) J Adhesion Sci Technol 11:1513
45. Babonneau F (1994) Polyhedron 13:1123
46. Peña-Alonso R, Téllez L, Rubio F, Rubio J (2006) J Sol-Gel Sci Tech 38:133
47. Saint-Flour C, Papirer E (1983) J Colloid Interface Sci 91:69
48. Belot V, Corriu RJP, Leclercq D, Mutin PH, Vioux A (1992) J Polymer Sci A 30:613
49. Sorarù GD, Liu Q, Interrante LV, Apple T (1998) Chem Mater 10:4047
50. Bois L, Maquet J, Babonneau F (1994) Chem Mater 6:796
51. Nawrocki J (1991) Chromatographia 31:177
52. Morrison SR (1977) The chemical physics of surfaces. Plenum Press, New York
53. Bogillo VI, Shkilev VP, Voelkel A (1996) Adsorption Sci Technol 14:189